

# A possible architecture of the planetary system HR 8799

Martin Reidemeister<sup>1</sup>, Alexander V. Krivov<sup>1</sup>, Tobias O. B. Schmidt<sup>1</sup>, Simone Fiedler<sup>1</sup>, Sebastian Müller<sup>1</sup>,  
Torsten Löhne<sup>1</sup>, and Ralph Neuhäuser<sup>1</sup>

Astrophysikalisches Institut, Friedrich-Schiller-Universität Jena, Schillergäßchen 2–3, 07745 Jena, Germany

Received *March 12, 2009*; accepted *May 20, 2009*

## ABSTRACT

HR8799 is a nearby A-type star with a debris disk and three planetary candidates recently imaged directly. We undertake a coherent analysis of various portions of observational data on all known components of the system, including the central star, imaged companions, and dust. The goal is to elucidate the architecture and evolutionary status of the system. We try to further constrain the age and orientation of the system, orbits and masses of the companions, as well as the location of dust. From the high luminosity of debris dust and dynamical constraints, we argue for a rather young system’s age of  $\lesssim 50$  Myr. The system must be seen nearly, but not exactly, pole-on. Our analysis of the stellar rotational velocity yields an inclination of  $13 - 30^\circ$ , whereas  $i \geq 20^\circ$  is needed for the system to be dynamically stable, which suggests a probable inclination range of  $20 - 30^\circ$ . The spectral energy distribution, including the Spitzer/IRS spectrum in the mid-infrared as well as IRAS, ISO, JCMT and IRAM observations, is naturally reproduced with two dust rings associated with two planetesimal belts. The inner “asteroid belt” is located at  $\sim 10$  AU inside the orbit of the innermost companion and a “Kuiper belt” at  $\geq 100$  AU is just exterior to the orbit of the outermost companion. The dust masses in the inner and outer ring are estimated to be  $\approx 1 \times 10^{-5}$  and  $4 \times 10^{-2}$  Earth masses, respectively. We show that all three planetary candidates may be stable in the mass range suggested in the discovery paper by Marois et al. 2008 (between 5 and 13 Jupiter masses), but only for some of all possible orientations. For  $(M_b, M_c, M_d) = (5, 7, 7)$  Jupiter masses, an inclination  $i \geq 20^\circ$  is required and the line of nodes of the system’s symmetry plane on the sky must lie within  $0^\circ$  to  $50^\circ$  from north eastward. For higher masses  $(M_b, M_c, M_d)$  from  $(7, 10, 10)$  to  $(11, 13, 13)$ , the constraints on both angles are even more stringent. Stable orbits imply a double (4:2:1) mean-motion resonance between all three companions. We finally show that in the cases where the companions themselves are orbitally stable, the dust-producing planetesimal belts are also stable against planetary perturbations.

**Key words.** planetary systems: formation – circumstellar matter – celestial mechanics – stars: individual: HR 8799.

## 1. Introduction

HR 8799 is an A5V star located at  $\approx 40$  pc away from Earth, around which three planetary candidates<sup>1</sup> have recently been imaged (Marois et al. 2008). All three objects have been shown to be co-moving with the star. For two of them, also a differential proper motion consistent with the orbital motion of a companion around the star has been detected. The presence of the outermost companion has recently been confirmed by Lafrenière et al. (2009) through analysis of archival HST/NICMOS data from 1998 and by Fukagawa et al. (2009) with SUBARU/CIAO data from 2002. No further companions with masses greater than  $3M_{\text{Jup}}$  (Jupiter masses) within 600 AU from the star have been found (Close & Males 2009). Three imaged companions are located at projected distances from 24 to 68 AU from the star and presumably have masses of the order of 7–10 Jupiter masses, although the mass determination is based solely on untested evolutionary models and an assumption that the system’s age lies in the range 30–160 Myr. First dynamical analyses (Fabrycky & Murray-Clay 2008; Goździewski & Migaszewski

2009) show that, with the current estimates of planetary masses and the assumption that true orbital separations of the planets are close to projected distances, the stability of the system on timescales comparable to the stellar age is not obvious. Still, the system can be stable, as it likely is, for instance if the planets are locked in resonances and/or the planetary masses are lower than estimated.

Apart from planets, HR 8799 has long been known to harbor cold circumstellar dust responsible for excess emission in the far-infrared discovered by IRAS (Sadakane & Nishida 1986; Zuckerman & Song 2004; Rhee et al. 2007). The rather strong infrared excess has been also confirmed with ISO/ISOPHOT measurements (Moór et al. 2006). Additionally, Spitzer/IRS measurements revealed warm dust emission in the mid-infrared (Jura et al. 2004; Chen et al. 2006). Both cold and warm dust emission must be indicative of one or more dust-producing planetesimal belts, similar to the Edgeworth-Kuiper belt and possibly, the asteroid belt in the solar system. Altogether, there appears to be an emerging view of a complex, multi-component planetary system with several planets, planetesimal belts, and dust.

Given the fact that the planets have been discovered very recently, it is not surprising that our knowledge of the system is very poor and that even the key parameters of the system and its components remain vaguely known. A large uncertainty in the system’s age amplifies the difficulty of inferring accurate masses of the companions from evolutionary models, and the mass estimates vary from one model to another even for the same age. While there are clear indications that the system is seen nearly

Send *offprint requests* to: A.V. Krivov, e-mail: krivov@astro.uni-jena.de

<sup>1</sup> For the sake of brevity, we often call them “planets” throughout this paper. This comes with the warning that the often used definition of an “extrasolar planet” as a star-orbiting body with mass under the deuterium burning limit remains controversial. Furthermore, it is not possible at present to completely exclude the possibility that the mass of at least one companion in the HR8799 system lies above that limit, although this appears rather unlikely.

pole-on, the exact orientation of its symmetry plane is not known either, which makes it impossible to convert projected astrometric distances of planets into their true positions. The differential proper motion was measured with a reasonable accuracy only for the outer planets, and even in that case the accuracy is not yet sufficient to constrain orbital eccentricities. As far as the dust is concerned, the debris disk remains unresolved, offering no possibility to better recover the orientation of the system’s plane. Even the photometry data are scarce. This results in a poor knowledge of the dust distribution.

Obviously, most of these issues could only be resolved with new observational data, some of which may come promptly, while some others may require longer time spans. However, already at the current stage, we find it reasonable to reanalyze the available data. While the discovery paper by Marois et al. (2008) mostly concentrates on the planets themselves and the first “follow-up” publications (Fabrycky & Murray-Clay 2008; Goździewski & Migaszewski 2009) provide an in-depth analysis of dynamical stability issues, in this paper we try to paint a more synthetic view of the planetary system around HR 8799 with all its components — central star, planets, and dust-producing planetesimal belts.

Section 2 focuses on the stellar properties, notably the stellar age (section 2.1) and inclination of the rotation axis, assumed to coincide with the inclination of the whole system (section 2.2). In Section 3, we analyze the observed spectral energy distribution (SED, section 3.1) and try to fit the data with several dust belts (section 3.2). Section 4 treats presumed planets and tries to constrain their masses both from evolutionary models (section 4.1) and dynamical stability requirement (section 4.2). Section 5 checks whether planetesimal belts, as found to fit the infrared photometry, would be dynamically stable against planetary perturbations. Section 6 contains our conclusions and a discussion.

## 2. The central star

### 2.1. Age

Marois et al. (2008) give an age of 30 to 160 Myr for HR 8799 and hence its companions, considering several age indicators. While most of the indicators support a rather younger age, few of them still allow for an older age or even suggest it. One indicator is the galactic space motion (UVW) of the primary, which is similar to that of close young associations (Marois et al. 2008). Using these data, Moór et al. (2006) propose HR 8799 to be a member of the Local Association at an age of 20 to 150 Myr with a probability of 62%. Another method is the position of HR 8799 in the Hertzsprung-Russell diagram. Taking into account the low luminosity of the star (after correction for its low metallicity) as well as the UVW space motion, Rhee et al. (2007) arrived at an age of 30 Myr.

Marois et al. (2008) further note that  $\lambda$  Bootis stars are generally thought to be young, up to a few 100 Myr. However, the Hipparcos mission has shown that the well established  $\lambda$  Bootis stars of the Galactic field comprise the whole range from the Zero Age Main Sequence to the Terminal Age Main Sequence, which is  $\sim 1$  Gyr for an A-type star (Turcotte 2002; Paunzen 2001, and references therein). The best indicator for a rather older age is the location of HR 8799 in a  $T_{\text{eff}}$  vs.  $\log g$  diagram derived from published uvby $\beta$  photometry. Using this method, Song et al. (2001) find an age of 50 to 1128 Myr with a best estimate of 732 Myr and Chen et al. (2006) an age of 590 Myr.

An independent argument in favor of a rather younger age may come from the the dust portion of the system. The mea-

sured infrared excess ratio of  $\sim 100$  at  $60\text{--}90\mu\text{m}$  (see Fig. 1 below) would be typical of a debris disk star with the age of  $\lesssim 50$  Myr (see Su et al. 2006, their Fig. 5). However, this argument is purely statistical and must be taken with caution. For instance, one cannot exclude the possibility that the formation of such a planetary system with three massive planets in very wide orbits could trace back to an exceptionally dense and large protoplanetary disk. The latter might leave, as a by-product, a more massive debris disk on the periphery, whose fractional luminosity might be well above the statistically expected level.

Altogether, there seem to be more arguments to advocate a younger age of the system of the order of several tens of Myr. On any account, as pointed out in the discovery paper by Marois et al. (2008) and is further discussed in section 4 below, extremely old ages would inevitably imply high object masses in the brown dwarf range — for all the evolutionary models used to infer the masses. Fabrycky & Murray-Clay (2008) have shown that dynamical stability of such a system is problematic. It can be stable for masses up to 20 Jupiter masses, but only for very special orbital configurations.

### 2.2. Rotational period and inclination

As summarized by Sadakane (2006) the Vega-like,  $\gamma$  Doradus type pulsator HR 8799 is showing  $\lambda$  Bootis-like abundances. He concludes that for the case of HR 8799, which is known to be a single star and associated with a dusty disk, the scenario invoking the process of selective accretion of circumstellar or interstellar material depleted in refractory elements, seems to be the favorable explanation for the unusually low abundances.

The fact that HR 8799 is a  $\gamma$  Doradus type pulsator makes it hard to find an indisputable rotational period. However, several authors give a value of  $\sim 0.51$  days (e.g. Rodriguez & Zerbi 1995). Zerbi et al. (1999) found from a multisite campaign three independent frequencies (0.5053 d, 0.5791 d, 0.6061 d) and a coupling term between them (4.0339 d). All of these frequencies could be independent pulsational modes. However, if one of these frequencies corresponds to the rotational period of the star, we are able to calculate the inclination  $i$  of its rotational axis.

From the possible rotational frequencies (0.5053 d, 0.5791 d, 0.6061 d) and from the radius of HR 8799 of  $1.32R_{\odot}$  (Allende Prieto & Lambert 1999) to  $1.6R_{\odot}$  (Pasinetti Fracassini et al. 2001), we determine the possible range of the true rotational velocity  $v$  of the star of  $110\text{--}160\text{ km s}^{-1}$ . These values agree quite well with the median  $v \sin i$  of A4–A6 main sequence stars of  $159 \pm 7.2\text{ km s}^{-1}$  (Royer et al. 2007). On the other hand, the projected rotational velocity  $v \sin i$  of HR 8799 was measured by several authors to be between  $35.5\text{ km s}^{-1}$  and  $55\text{ km s}^{-1}$  (e.g. Kaye & Strassmeier 1998; Uesugi & Fukuda 1982). From  $v$  and  $v \sin i$ , we finally derive a possible range of the inclination of the star of  $13^{\circ}\text{--}30^{\circ}$ . Note that in the above estimates we excluded the 4.0339-day period as this would lead to  $\sin i > 1$ .

It can be expected that the rotational equator of the star and the planetary orbits are all aligned with each other. Spin-orbit alignment is a common assumption, consistent for instance with the data of most transiting planets (e.g. Fabrycky & Winn 2009). It has also been confirmed for Fomalhaut and its disk (Le Bouquin et al. 2009). Nonetheless, a misalignment on the order of several degrees is likely. It is exemplified by our own system, in which the Jupiter orbit is tilted by  $\sim 7^{\circ}$  to the solar equator and the orbital planes of giant planets differ from each other by a few degrees. With this caveat, we make an assumption of the perfect alignment throughout the paper. This assumption

is particularly needed to reduce the complexity of our dynamical stability studies presented below.

An additional argument in favor of a low inclination of the whole system comes from the fact that the measured proper motion of the companions relative to the star is also consistent with a nearly pole-on view onto the system (Marois et al. 2008). The most recent astrometric analysis by Lafrenière et al. (2009) further supports this conclusion. Their best fits with circular orbits suggest the semimajor axis  $a \sim 68\text{--}74$  AU and the inclination  $i \sim 13^\circ\text{--}23^\circ$  for the orbit of the outermost companion, HR 8799 b.

### 3. Dust and planetesimal belts

#### 3.1. Observed SED

Table 1 lists the catalogs and references used to provide the optical, infrared, sub-mm and millimeter photometry. We employed the Hipparcos and Tycho databases as well as USNO and GSC catalogs to compile the optical photometry, whereas the near-infrared data were taken from the 2MASS survey. The mid- and far-infrared photometry is provided by the IRAS and ISO satellites, while sub-mm and millimeter data were obtained at JCMT and IRAM. For transforming the  $B$ ,  $V$ ,  $R$ ,  $I$  magnitudes into units of flux [Jy] we used the standard calibration system of Johnson, whereas in case of the 2MASS  $J$ ,  $H$ ,  $K_s$  bands the calibrations of Cohen et al. (2003) were applied. For the IRAS fluxes a color-correction factor (Beichman et al. 1988) assuming a black body spectral energy distribution for a temperature of 5000 K was employed<sup>2</sup>.

The optical and near-infrared photometry was used to derive a best-fit photospheric model. We estimated the stellar photospheric fluxes by minimum  $\chi^2$  fitting of NextGen model atmospheres (Hauschildt et al. 1999), using only bandpasses with wavelengths shorter than  $3\ \mu\text{m}$ , where no excess emission is expected. In our search for the best fit we employed a system of NextGen models with an effective temperature step size of 200 K, with a  $\log g$  of 4.5, and with solar metallicity<sup>3</sup>. Varying the temperature as well as the stellar radius, which affects the solid angle dilution factor, we derive a best-fit temperature of 7400 K and a best-fit radius of  $1.34 R_\odot$ , both in a very good agreement with the results of Gray & Kaye (1999).

In order to obtain more information on the dust component of the system, we extracted publicly available IRS data for HR8799 from the Spitzer archive with the Leopard software (<http://ssc.spitzer.caltech.edu/irs/>). Those data were taken in December 2003 under AOR 3565568 and originally published by Chen et al. (2006). Using the post-basic correction data provided by the standard IRS pipeline, we first subtracted the zodiacal light background estimated by the SPOT software. Then we joined the datasets for the individual IRS modules and orders and subtracted a simple Rayleigh-Jeans stellar photosphere in the wavelength region of interest, assuming now that there is no excess at  $8\ \mu\text{m}$  where the IRS spectrum starts. For plotting and fitting purposes, the scatter in the resulting dust spectrum was reduced by taking averages over 4 neighboring data points. This increases the signal-to-noise ratio without lowering the spectral resolution, which remains constrained by the instrumental value  $R \sim 60\text{--}120$ . Spurious features at the edges of the spectral orders around  $14$  and  $20\ \mu\text{m}$  were removed.

<sup>2</sup> Correction factors are only available over a coarse temperature grid ..., 5000 K, 10000 K.

<sup>3</sup> Although the metallicity of HR8799 is  $-0.47$  (Gray & Kaye 1999), this parameter has no important effect on the fitting result.

The resulting spectrum shows a somewhat (by  $\approx 40\%$ ) weaker excess than that by Chen et al. (2006), especially between  $20$  and  $30\ \mu\text{m}$ . One possible origin of this discrepancy is the approach used for background subtraction. In addition, both spectra fall well below the IRAS upper limits at  $25\ \mu\text{m}$  but also by several  $\sigma$  below the IRAS  $12\ \mu\text{m}$  faint-source and point-source measurements. The easiest way to reduce this scaling uncertainty would be using a good photometry point in the mid-infrared. Unfortunately, a  $24\ \mu\text{m}$  Spitzer/MIPS point, which would ideally serve for this purpose, is not yet available in the Spitzer archive, although these data have recently been taken (Kate Su, pers. comm). Whether the maximum at around  $11\ \mu\text{m}$  is a silicate feature is unclear. Definite conclusions would require a longer exposure time and a higher spectral resolution.

The resulting set of photometry points and the IRS spectrum are shown in Fig. 1 (with photosphere) and in Fig. 2 (excess emission only).

**Table 1.** Photometry of HR8799. IRAS fluxes are color corrected as described in the IRAS Explanatory Supplement (Beichman et al. 1988).

Photometric band	Flux or magnitude	$F_{qual}$ (IRAS)	Ref.
	[mag]		
$B$	$6.090 \pm 0.300$		(1)
$B$	6.196		(2)
$B$	$6.210 \pm 0.010$		(3)
$B$	$6.214 \pm 0.009$		(4)
$V$	$5.960 \pm 0.010$		(4)
$V$	5.959		(2)
$V$	$5.960 \pm 0.010$		(3)
$R$	$5.810 \pm 0.300$		(1)
$I$	$5.690 \pm 0.300$		(1)
$J$	$5.383 \pm 0.027$		(5)
$H$	$5.280 \pm 0.018$		(5)
$K_s$	$5.240 \pm 0.018$		(5)
	[Jy]		
IRAS PSC $12\ \mu\text{m}$	$0.267 \pm 0.034$	3	(6)
IRAS PSC $25\ \mu\text{m}$	$0.246 \pm 0.000$	1	(6)
IRAS PSC $60\ \mu\text{m}$	$0.307 \pm 0.061$	2	(6)
IRAS PSC $100\ \mu\text{m}$	$2.376 \pm 0.000$	1	(6)
IRAS FSC $12\ \mu\text{m}$	$0.278 \pm 0.036$	3	(7)
IRAS FSC $25\ \mu\text{m}$	$0.174 \pm 0.075$	1	(7)
IRAS FSC $60\ \mu\text{m}$	$0.311 \pm 0.062$	3	(7)
IRAS FSC $100\ \mu\text{m}$	$3.202 \pm 0.977$	1	(7)
ISO $60\ \mu\text{m}$	$0.412 \pm 0.021$		(8)
ISO $90\ \mu\text{m}$	$0.585 \pm 0.041$		(8)
	[mJy]		
JCMT $850\ \mu\text{m}$	$10.3 \pm 1.8$		(9)
JCMT $1100\ \mu\text{m}$	< 33		(10)
IRAM $1200\ \mu\text{m}$	$4.8 \pm 2.7$		(10)

References: (1) The USNO-B1.0 Catalog (Monet et al. 2003); (2) NOMAD Catalog (Zacharias et al. 2004), from Tycho-2 Catalog (Høg et al. 2000); (3) The Guide Star Catalog, Version 2.3.2 (Lasker et al. 2008); (4) The Hipparcos and Tycho Catalogues (Perryman & ESA 1997); (5) 2MASS All-Sky Catalog of Point Sources (Skrutskie et al. 2006); (6) IRAS catalogue of Point Sources, Version 2.0 (Helou & Walker 1988); (7) IRAS Faint Source Catalog,  $|b| > 10$ , Version 2.0 (Moshir et al. 1990); (8) (Moór et al. 2006) (9) (Williams & Andrews 2006) (10) (Sylvester et al. 1996)

#### 3.2. Interpretation

To get a rough idea of the location of the dust belt(s) and the amount of dust in the HR8799 system, we modeled the SED assuming a double power-law surface number density of dust  $N \propto s^{-q}r^{-\xi}$ , where  $s$  and  $r$  are the dust grain size and distance

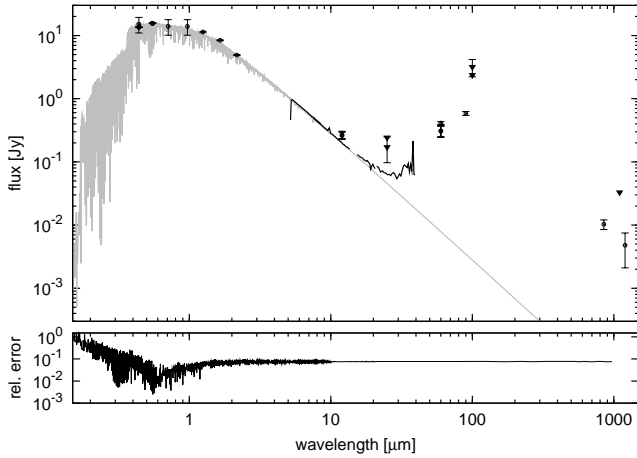


**Fig. 1.** Spectral energy distribution of HR 8799. Circles are photometric measurements, triangles are upper limits (Table 1). The black line between  $\approx 5$  and  $40 \mu\text{m}$  is the Spitzer/IRS spectrum. Overlaid is the best-fit NextGen model (grey line) for the stellar photosphere. Its estimated relative error is plotted under the main panel.

**Table 2.** Locations and names of the first-guess dust rings.

ring location	ring extension [AU]	name
inside d	3 – 15	ring d
between d and c	28 – 32	ring cd
between c and b	45 – 60	ring bc
outside b	75 – 125	ring b

from the star, respectively. Keeping in mind that SED interpretation is a degenerate problem and to decrease the number of free parameters, we restrict ourselves to the case of  $q = 3.5$  and  $\xi = 1$ . The dust composition was assumed to be astronomical silicate (Laor & Draine 1993). As the minimum grain size, we chose the radiation pressure blowout radius, which amounts to  $\approx 5 \mu\text{m}$  for astrosilicate. The maximum grain radius, which has little effect on the results, was arbitrarily set to  $1000 \mu\text{m}$ .

At first, we modeled the SEDs that would arise from four hypothetical dust rings with arbitrarily chosen extensions, located inside the orbit of the innermost planet HR8799 d, between d and c, between c and b, and outside the orbit of the outermost planet HR8799 b (Table 2). Dust masses were chosen in such a way as to reproduce the  $60 \mu\text{m}$  flux. The results are shown in Fig. 2.

Comparison of the first-guess model SEDs with the available photometry and spectrometry observations reveals two issues. First, one single ring is not capable of reproducing the entire set of observations from the mid- to the far-infrared. Second, if the  $10 \mu\text{m}$  silicate feature in the IRS spectrum is real, a substantial fraction of particles smaller than the blowout size will be required.

Taking these discrepancies into account, we combined two rings, ‘ring d’ and ‘ring b’, and fitted the lower size cutoffs and dust masses to the observations. In our ‘best fit’ model, which is shown as solid line in Fig. 2, the minimum sizes are 2 and  $6 \mu\text{m}$  and the dust masses are  $1.4 \times 10^{-5} M_{\oplus}$  and  $4.2 \times 10^{-2} M_{\oplus}$  for the inner and outer ring, respectively. As a word of caution, we remind that these estimates directly inherit the uncertainty of the

IRS spectrum calibration, as discussed in section 3.1, which is a factor of several in dust mass.

A question arises whether these fits are physically reasonable. In particular, it is not immediately clear whether the blowout particles are really needed to reproduce the observations. Similar problems have already been encountered in studies of other debris disks (e.g. around Vega, see Su et al. 2005). However, such inconsistencies can be overcome by considering a complete dynamical treatment of the specific disk without significant changes in the disk location (Müller et al., in prep.). Further, our choice of power-law spatial and size distributions is only a rough, albeit commonly used, approximation. More elaborate dynamical studies (e.g. Krivov et al. 2006; Thébaud & Augereau 2007) show clear deviations from this assumption, especially in the case of the dust size distribution where a wavy pattern arises from an underabundance of small particles induced by radiation blowout. Thus, we checked the impact of moderate variations in the slopes ( $0.1 \leq \xi \leq 1.9$  and  $2.5 \leq q \leq 4.5$ ). It turned out that the slope of the spatial distribution  $\xi$  has little effect on the results, moderately changing only the short-wavelength part in the SED from the inner dust ring. The size distribution slope  $q$ , however, affects the resulting emission appreciably. While for the inner ring the changes are still small (a steeper slope would amplify the silicate features at 10 and  $20 \mu\text{m}$  whereas a shallower distribution would wash them out, just as expected), similar changes in the outer ring would require a strong compensation by altering other disk parameters (which were fixed in our approach). The reason is that for the outer component both the rise and the fall of the SED are well constrained by photometric observations. They place tight constraints on the width of the SED, in contrast to the inner ring where only the short-wavelength part of the SED is known. Since dust in the outer ring is much colder than in the inner ring it is no longer the strength of the features but the width of the SED that is affected by a different slope in the size distribution: the steeper the distribution, the narrower the SED. On any account, for our purpose of determining the rough location and mass of dust the simple fitting approach used here is sufficient.

Another question is, how well the edges of the outer and inner ring are constrained. To check this, we varied them and fitted the SED again, leaving the lower cutoff size and dust mass as free parameters. For the outer ring, we found reasonable fits with the inner edge between 75 and 120 AU and the outer edge between 125 and 170 AU (for  $q = 3.5$  and  $\xi = 1$ ). The outer edge in the inner ring can go from 15 down to 10 AU. In fact, the inner ring truncated at 10 AU provides even slightly better agreement with the IRS spectrum between 20 and  $30 \mu\text{m}$ . However, due to the calibration uncertainties it is difficult to assess the accuracy of the fit, which leaves the outer edge of the inner ring rather unconstrained. The inner edge of the inner ring can be as close to the star as 2 AU to conform to the IRS spectrum.

So far we have discussed *dust* rings in the system. However, the presence of a dust belt requires a belt of *planetesimals* that do not show up in the observations, but produce and sustain visible dust. Due to the radiation pressure effect, dust grains typically move in orbits with periastra at the planetesimal belt and apastron outside it. The smaller the grains, the farther out from the star they are spread. Thus the dust-producing planetesimal belt is expected to be narrower than the observed dust ring and to lie within the dust ring close to its inner edge (e.g. Krivov et al. 2006). Therefore, we can expect that the outer planetesimal belt is located at  $\sim 75$ –120 AU and the inner planetesimal belt at 2–10 AU from the star. It is important to check whether the expected locations of the outer and inner planetesimal belt are dy-

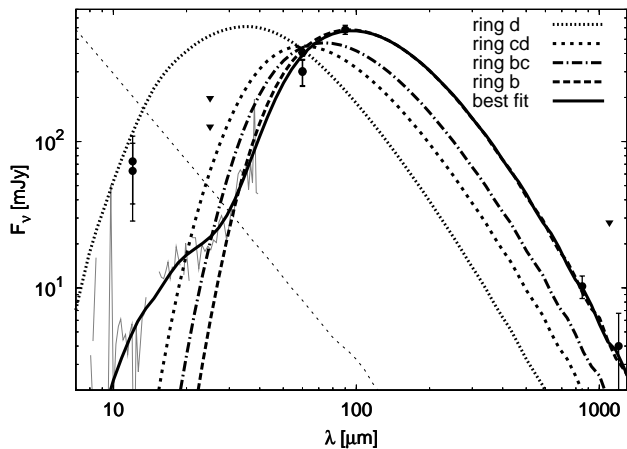


**Fig. 2.** Excess emission of HR 8799 in the infrared. The grey solid line is the IRS spectrum. The circles are the observed fluxes, and the triangles are upper limits. Dotted, short-dashed, dash-dotted, and long-dashed lines are the SEDs from the four first-guess dust rings (Table 2). The black solid line is our ‘best fit’.

namically compatible with the presence of the outermost and innermost planet, respectively. We will investigate this in section 5, trying to find additional constraints on the location of the two rings.

## 4. Planets

### 4.1. Masses from models

A common method to estimate masses of various astrophysical objects, from stars to planets, is to use their formation and evolution models. Such models predict essential physical parameters of objects of various masses, notably their luminosity and temperature, as a function of age. If the age is known, a comparison with luminosity or temperature retrieved from observations allows one to estimate the mass. In the case of HR8799, the temperature of the companions is unknown, but their luminosity has been derived from brightness and distance with sufficient accuracy to apply the models. Ages, masses, and other parameters of other directly imaged planet candidates were recently reviewed by Schmidt et al. (2009).

However, all models involve simplifying assumptions and adopt certain initial conditions, e.g. the initial internal energy and temperature structure. Further, the so-called hot-start models all start at a non-zero age (e.g., 0.1 or 1 Myr) with a finite luminosity and thus do not cover the actual formation stage. For these reasons, models may not deliver reliable results for at least the first several Myrs (see Wuchterl 2001; Chabrier et al. 2005, for discussion), if not several hundred Myrs (Stevenson 1982).

Using the model by Baraffe et al. (2003) and assuming the age range of 30–160 Myr, Marois et al. (2008) estimated the masses of companions to be  $7M_{\text{Jup}}$  ( $5\text{--}11M_{\text{Jup}}$ ) for HR8799 b and  $10M_{\text{Jup}}$  ( $7\text{--}13M_{\text{Jup}}$ ) for HR 8799 c & d. We have recalculated possible masses of the three companions with the aid of several state-of-the-art hot-start evolutionary models from system’s age and companions’ luminosity. In so doing, we allowed a broader range of possible ages, as discussed in section 2.1. Table 3 shows the results. Note that some models give masses only for limited age and/or mass ranges; for instance, the model by Marley et al.

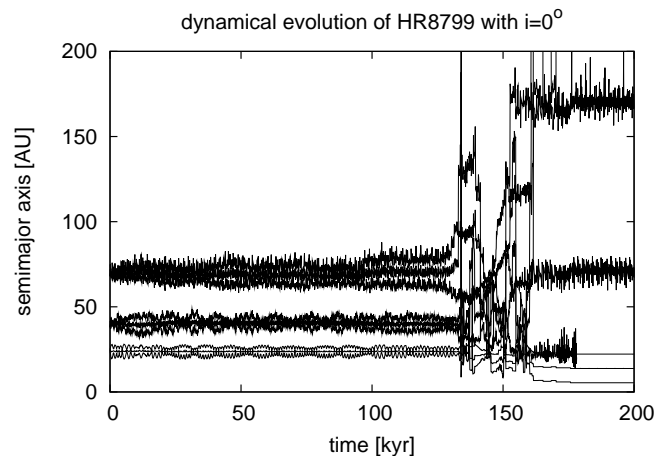


**Fig. 3.** Instability of the planetary system with nominal masses in the non-inclined case. For each of the planets, three curves correspond to semimajor axes, pericentric distance, and apocentric distance.

(2007) does not go beyond  $10M_{\text{Jup}}$ . This explains why some positions in the table are not filled.

On the whole, the mass estimates we obtain are similar to those by Marois et al. (2008). The ages above  $\sim 160$  Myr would lead to “non-planetary” masses above the standard deuterium burning limit of  $13.6M_{\text{Jup}}$ . On the other hand, none of the models predict masses below 3 – 5 ( $\text{HR8799 b}$ ) and 6 – 8 ( $\text{HR8799 c, d}$ ) Jupiter masses even for the youngest plausible ages of  $\sim 20$  Myr.

### 4.2. Masses from stability requirement

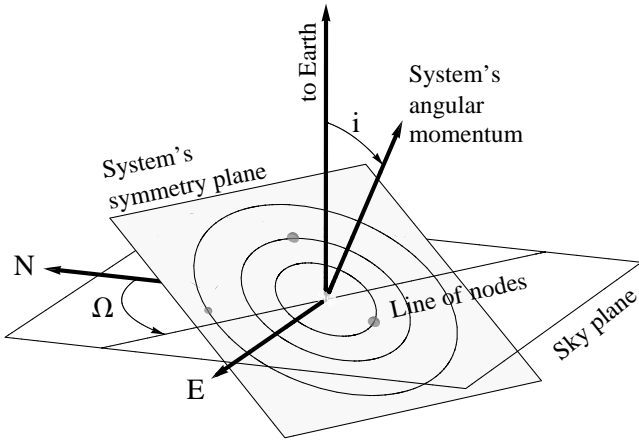
The simplest possible assumption one can make is that the system is seen perfectly face-on (inclination  $i = 0$ ) and that all three planets are initially in circular, co-planar orbits. However, as Fabrycky & Murray-Clay (2008) pointed out, such a system with masses reported in Marois et al. (2008) would be unstable. This is readily confirmed by our numerical integrations that are described below. Fig. 3 shows the time evolution of the planetary orbits; already after 134 kyr a close encounter between HR8799 c and d occurs and triggers instability of all three planets ending with the ejection of HR8799 c 50 kyr later. These timescales are fully consistent with those reported by Fabrycky & Murray-Clay (2008).

The studies by Fabrycky & Murray-Clay (2008) and Goździewski & Migaszewski (2009) were largely based on fitting simultaneously the observed positions and differential proper motion of the companions and checking the stability of the resulting systems in the course of their dynamical evolution. Noting that constraints on eccentricities from the differential proper motion are rather weak, but clear indications exist for inclined orbits from the rotational period analysis (see section 2.2), here we employ a different method. We confine our simulations to initially circular orbits (and let the eccentricities evolve to non-zero values at later times), but allow the symmetry plane to have all conceivable non-zero inclinations and an arbitrary orientation. Thus, for the subsequent analysis we introduce two angles (Fig. 4). One is the inclination  $i$  itself, measured between the angular momentum vector and a vector pointing toward the observer. Another angle is the longitude of node  $\Omega$  of the system’s symmetry plane on the plane of the sky, which is measured from north in the eastern direction. We vary the inclination  $i$  from

**Table 3.** Masses of HR 8799 b / c / d from luminosity (and absolute K-band magnitude) using various evolutionary models.

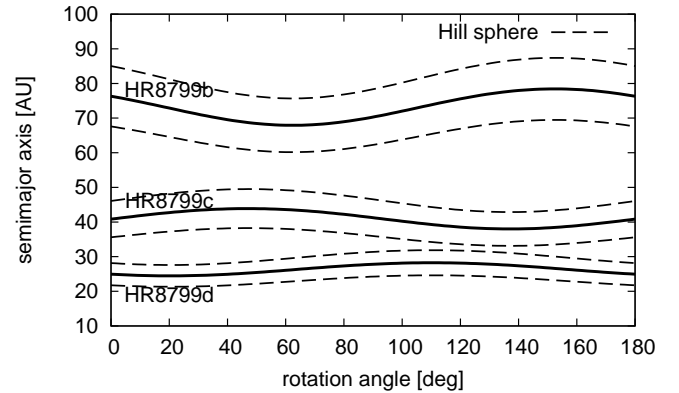
HR8799 b		Luminosity $\log L/L_{\odot} = -5.1 \pm 0.1$ (Marois et al. 2008)								
Model	Mass [ $M_{\text{Jup}}$ ] at age									
	20 Myr	30 Myr	60 Myr	100 Myr	160 Myr	590 Myr	730 Myr	1000 Myr	1128 Myr	
Burrows et al. (1997)	3.5 – 4.5	4.5 – 6	7 – 8.5	9 – 11	11.5 – 12.5	22 – 26	25 – 30	28 – 33	30 – 36	
Marley et al. (2007) <sup>a</sup>	3 – 5	4 – 7	6 – 10							
Chabrier et al. (2000)						21 – 26		30 – 35		
Baraffe et al. (2003)		4 – 5	6 – 7	9 – 10		21 – 26		30 – 35		
Baraffe et al. (2008) <sup>b</sup>			~ 7	~ 9						
Baraffe et al. (2003) <sup>c</sup>		~ 5.5	~ 8.5	~ 10.5		~ 30		~ 38		
HR8799 c / d		Luminosity $\log L/L_{\odot} = -4.7 \pm 0.1$ (Marois et al. 2008)								
Model	Mass [ $M_{\text{Jup}}$ ] at age									
	20 Myr	30 Myr	60 Myr	100 Myr	160 Myr	590 Myr	730 Myr	1000 Myr	1128 Myr	
Burrows et al. (1997)	6 – 7.5	7.5 – 9.5	11 – 12	12.5 – 13	13 – 13.5	30 – 38	35 – 43	40 – 48	41 – 50	
Marley et al. (2007) <sup>a</sup>	6 – 8	8 – 10								
Chabrier et al. (2000)		6 – 7	8 – 10	10 – 11		28 – 34		39 – 46		
Baraffe et al. (2003)		6 – 7	8 – 10	10 – 11		27 – 31		37 – 43		
Baraffe et al. (2008) <sup>b</sup>			~ 9							
Baraffe et al. (2003) <sup>d</sup>		~ 7.5	~ 10.5	~ 11.5		~ 38		~ 48		

Remarks: All mass values were shortened to appropriate decimals and partly rounded to halves or integers of a Jupiter mass. (a) Hot-start models. (b) Non irradiated models. (c) Using  $M_{K_s} = 14.05 \pm 0.08$  mag (Marois et al. 2008). (d) Using  $M_{K_s} \sim 13.12$  mag instead of slightly different values  $M_{K_s} = 13.13 \pm 0.08$  mag for HR8799 c and  $M_{K_s} = 13.11 \pm 0.12$  mag for HR8799 d, given in Marois et al. (2008).

**Fig. 4.** Orientation of the system with respect to the line of sight.

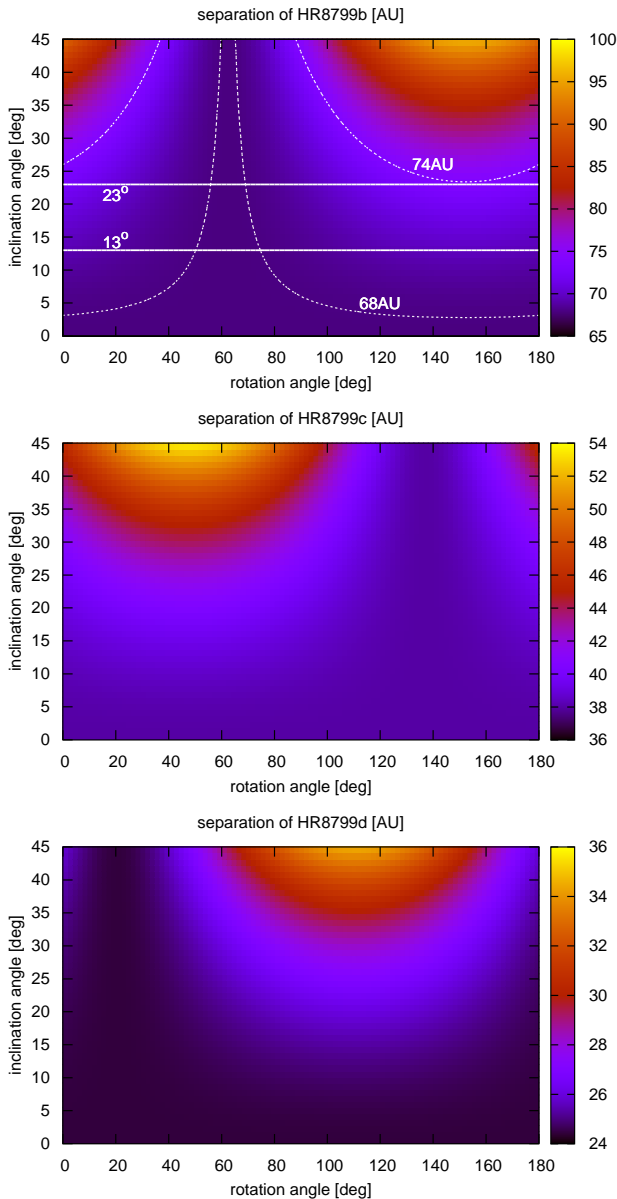
$0^\circ$  to  $45^\circ$ , thus extending the range suggested by section 2.2 to higher values. This may be useful to accommodate a possible tilt of planetary orbits to the stellar equator. The rotation angle  $\Omega$  is unconstrained by the observations. It is sufficient to vary it from  $0^\circ$  to  $180^\circ$ , since the true mutual positions of all three planets at  $(i, \Omega)$  and  $(i, \Omega + 180^\circ)$  would be exactly the same. For each  $(i, \Omega)$ -pair we can convert the observed (projected) instantaneous positions (astrometric distances and positional angles) of the three planets into their true positions in space. If, further, initially circular orbits are assumed, the calculated distances of planets will coincide with their initial semimajor axes. We thus consider a two-parametric  $(i, \Omega)$  set of possible systems; for each of them, the initial orbital configuration is fully and uniquely defined.

Fig. 5 shows the astrometric semimajor axes of the three planets with an inclination of  $i = 30^\circ$  as a function of rotation angle  $\Omega$ , as well as the corresponding Hill spheres for nominal planetary masses. Similarly, Fig. 6 depicts the initial semimajor axis of the planets depending on  $i$  and  $\Omega$ . Note that the recent

**Fig. 5.** Semimajor axes of HR8799b, c and d (solid lines) and their Hill radii for nominal masses (dashed) as a function of  $\Omega$  for  $i = 30^\circ$ .

analysis of HR8799 b by Lafrenière et al. (2009), which is based on the archival HST/NICMOS data from 1998, yielded a semimajor axis of  $a \sim 68\text{--}74$  AU and an inclination of  $i \sim 13^\circ\text{--}23^\circ$ . Finally, Fig. 7 plots the difference of initial semimajor axes of HR8799 b and c, as well as HR8799 c and d, again depending on  $i$  and  $\Omega$ . From all these figures, it is clearly seen that the orbital spacing, and therefore the stability, might indeed strongly depend on the orientation of the system.

This expectation is fully confirmed by the main bulk of numerical integrations that we performed with the aid of the MERCURY6 package (Chambers 1999). We used the hybrid symplectic/Bulirsch-Stoer integrator with an adaptive stepsize and a  $10^{-14}$  angular momentum conservation accuracy, which changes to Bulirsch-Stoer algorithm at distances less than 3 Hill radii. Output has been stored every 1000 years. Each integration terminated when two planets had a distance less than half the Hill radius or after an integration time of  $t_{\text{max}} = 100$  Myr. In all cases we assumed a stellar mass of  $1.5M_{\odot}$  and a distance of 39.4 pc to convert the separation angle into the projected as-



**Fig. 6.** Initial semimajor axes of HR8799b (*top*), c (*middle*) and d (*bottom*) as a function of  $i$  and  $\Omega$ . Solid horizontal lines in the uppermost panel border the range of inclination range of  $i = 13\text{--}23^\circ$  for HR8799 b, reported by Lafrenière et al. (2009). Dashed lines do the same for the semimajor axis range,  $a = 68\text{--}74$  AU.

trocentric distance. The three planets started at positions at the epoch of 2008 Sept. 18 (see Table 1 in Marois et al. 2008). We used 3 different sets of possible planet masses (see Table 4) and checked stability for  $i \in \{0, 1, \dots, 45^\circ\}$  and  $\Omega \in \{0, 5, \dots, 180^\circ\}$ . Note that, although we assumed initially circular orbits, it does not mean that the orbits stay circular at later times. Just the opposite: the mutual perturbations always force eccentricities to take values in the range between zero and approximately 0.1, so that the initial circularity is “forgotten” by the system.

The results of these integrations are presented in Fig. 8. It depicts the time interval until the first close encounter — as a proxy for stability — with an upper limit of 100 Myr. It is seen that all three planets may be stable for 100 Myr for either set of planetary masses, but only for some of all possible orienta-

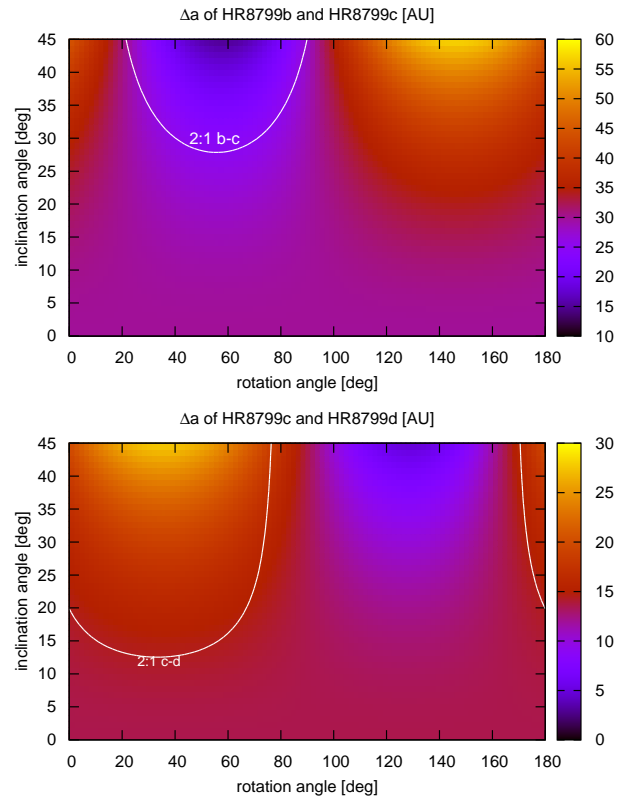


**Fig. 7.** Difference of initial semimajor axes  $\Delta a$  between HR8799 b & c (*top*) and HR8799 c & d (*bottom*) as a function of  $i$  and  $\Omega$ , as well as the location of the 2:1 commensurability of the periods for circular orbits.

**Table 4.** Three sets of planet masses used in numerical integrations

HR8799	b	c	d
low mass	$5M_{\text{Jup}}$	$7M_{\text{Jup}}$	$7M_{\text{Jup}}$
nominal mass	$7M_{\text{Jup}}$	$10M_{\text{Jup}}$	$10M_{\text{Jup}}$
high mass	$11M_{\text{Jup}}$	$13M_{\text{Jup}}$	$13M_{\text{Jup}}$

tions. Specifically, an inclination of  $\geq 20^\circ$  is required and the rotation angle  $\Omega$  must lie within the range from  $\approx 0^\circ$  to  $\approx 50^\circ$ . The higher the masses, the narrower the “stability spot” in the  $(i, \Omega)$ -plane. Further, we conclude that it is the inner pair (c and d) that tends to destroy the stability. Indeed, comparing Fig. 8 to Fig. 7 one sees that the most stable regions are those where  $\Delta a$  of HR8799 c and d is the largest, whereas that of HR8799 b and c is not. Finally, a comparison of Fig. 8 and Fig. 6 shows that the position of the “stability spot” in Fig. 8 roughly matches the inclination of  $i = 13\text{--}23^\circ$  and the semimajor axis of  $a = 68\text{--}74$  AU of the outermost planet reported by Lafrenière et al. (2009).

We now check whether all considered geometries are consistent with the measured differential proper motion of the companions. Fig. 9 depicts the projected differential proper motions  $\mu$  that the planets in circular orbits would have for each pair of  $i$  and  $\Omega$ . Overplotted are the values of  $\mu$  actually measured together with their  $1\sigma$  and  $2\sigma$  deviations. For HR8799 c, we used  $\mu = 30 \pm 2$  mas/yr from Marois et al. (2008). In contrast, for HR8799 b we derived the differential proper motion of  $22 \pm 2$  mas/yr by combining the Marois et al. measurements with

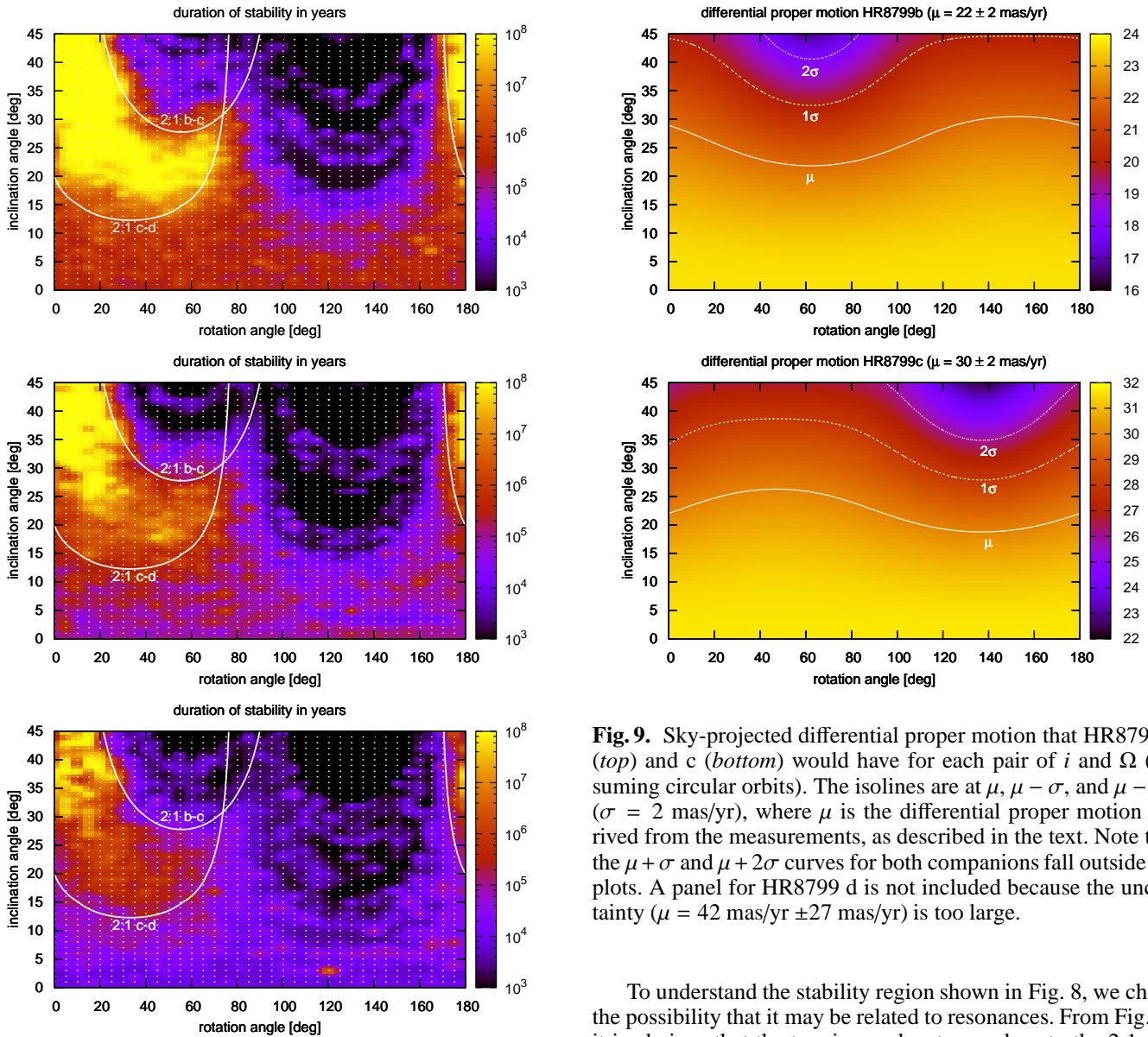


**Fig. 8.** Duration of stability depending on  $i$  and  $\Omega$  for different sets of planetary masses given in Tab. 4: *top*: low, *middle*: nominal, *bottom*: high. A grid of dots corresponds to the actual set of numerical runs (one dot = one run). Curves show where the periods between b-c and c-d would have a commensurability of 2:1 if the orbits were exactly circular.

the 1998 data from Lafrenière et al. (2009). Note that further adding the 2002 positions from Fukagawa et al. (2009) does not change this result. For comparison, the differential proper motion of HR8799 b given in Marois et al. (2008) is  $25 \pm 2$  mas/yr. In the non-inclined case, the calculated differential proper motion is always within  $1\sigma$  of the measured one. For HR8799 b, all orbits with an inclination  $< 33^\circ$  lie within  $1\sigma$  of the measured value. For HR8799 c, the same is true for  $i < 28^\circ$ . Nearly the whole parameter range of  $(i, \Omega)$  explored here is compatible with observations within  $2\sigma$ . It is easy to show that taking into account actual low eccentricities up to  $\approx 0.1$  acquired by the planets would not change this conclusion.

**Fig. 9.** Sky-projected differential proper motion that HR8799 b (*top*) and c (*bottom*) would have for each pair of  $i$  and  $\Omega$  (assuming circular orbits). The isolines are at  $\mu$ ,  $\mu - \sigma$ , and  $\mu - 2\sigma$  ( $\sigma = 2$  mas/yr), where  $\mu$  is the differential proper motion derived from the measurements, as described in the text. Note that the  $\mu + \sigma$  and  $\mu + 2\sigma$  curves for both companions fall outside the plots. A panel for HR8799 d is not included because the uncertainty ( $\mu = 42$  mas/yr  $\pm 27$  mas/yr) is too large.

To understand the stability region shown in Fig. 8, we check the possibility that it may be related to resonances. From Fig. 10 it is obvious that the two inner planets are close to the 2:1 resonance. With still coplanar and circular orbits, we looked for combinations of  $i$ ,  $\Omega$  that would correspond to the 2:1 commensurability. The resulting loci of the nominal 2:1 resonance in the  $(i, \Omega)$ -plane (Fig. 8) just encircle the stability region. This strengthens the hypothesis that the stability may be directly related to the 2:1 resonance.

We then checked whether or not the orbits of HR8799 c and d within the stability region are indeed locked in the resonance. To this end, we have calculated the resonant argument  $\varphi_{cd} = 2\lambda_c - \lambda_d - \omega_d$ , where  $\lambda_c$  and  $\lambda_d$  are the mean longitudes of HR8799 c and d and  $\omega_d$  is the argument of pericenter of the latter planet. We found that *all* stable orbits are indeed resonant. Interestingly, the initial values of  $\lambda_c$  and  $\lambda_d$  adopted in all numerical runs were such that the planets are not locked in the resonance initially, but — in all stable cases — the system swiftly “slips” into the resonance, which makes it safe. The resonant argument  $\varphi_{cd}$  librates around  $0^\circ$  with an amplitude (which we calculated as a standard deviation) of  $22^\circ$ – $100^\circ$ . For comparison, the non-resonant case would have a standard deviation of  $\sim 103.9^\circ$ . However, we made sure that even the cases with the libration amplitude up to  $100^\circ$  are resonanceces, albeit shallow. In these cases, the resonant argument circulates rather than librates.



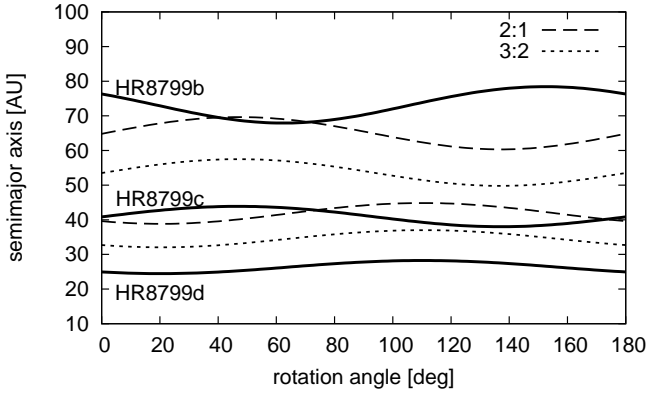


**Fig. 10.** Semimajor axes of HR8799b, c and d (solid lines) and positions of external 2:1 (dashed) and 3:2 nominal resonances (dotted) of two inner planets as a function of  $\Omega$  for  $i = 30^\circ$ .

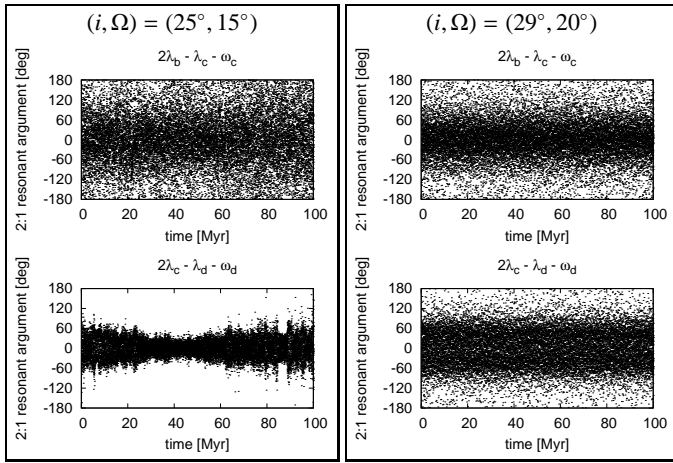


**Fig. 11.** Typical behavior of resonant arguments for the 2:1 mean motion resonance between HR8799 b & c (top) and HR8799 c & d (bottom). Nominal planetary masses are assumed. The libration amplitude is  $86^\circ$  (left top),  $36^\circ$  (left bottom),  $63^\circ$  (right top), and  $60^\circ$  (right bottom).

Thus the phase trajectories on the  $e_c \cos \varphi_{cd} - e_c \sin \varphi_{cd}$  plane are circles with an offset from (0,0), which is indicative of a resonant locking.

For all stable configurations we then calculated the resonant argument for the two outer planets, HR8799 b and c, defined as  $\varphi_{bc} = 2\lambda_b - \lambda_c - \omega_c$ . We found that they are in a 2:1 resonance, too, with the standard deviation in the range  $36^\circ$ – $97^\circ$ . Note that in all stable cases at least one of the resonances, c-d or b-d, is strong, as suggested by a low libration amplitude. Two typical examples of the time evolution of the resonant argument for both planetary pairs are shown in Fig. 11. Thus our results are consistent with those by Fabrycky & Murray-Clay (2008) and Goździewski & Migaszewski (2009), who suggested a double resonance 4:2:1 as the likely “survival recipe” for the entire three-planet system.

As noted above, the major danger of system’s destabilization comes from the two inner planets which are likely more massive and more tightly spaced. Keeping this in mind and taking into account that data on the innermost companion (e.g. its differential proper motion) are as yet the least reliable, we checked the dynamical stability properties the system would have without

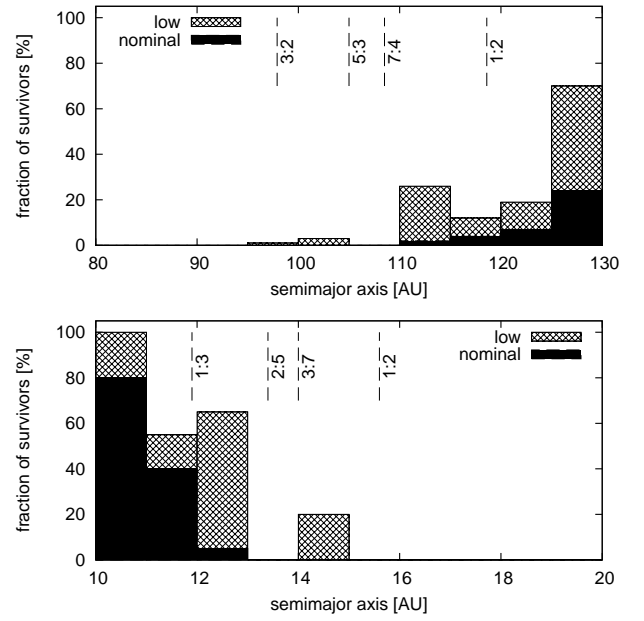


**Fig. 13.** Fraction of left-over planetesimals after 100 Myr of evolution in the outer (top) and inner (bottom) rings. Filled/hatched bars: nominal/low planetary mass.

HR8799 d. We used the same setup for MERCURY6 and restricted our analysis to three cases: non-inclined configuration,  $i = 15^\circ$ , and  $i = 30^\circ$ . The overall result is that, as expected, the absence of the inner companion would drastically improve stability:

- *The non-inclined configuration* becomes stable over a period of 100 Myr — not only for the nominal masses, but also for much higher masses up to  $M_b = 22M_{\text{Jup}}$  and  $M_c = 30M_{\text{Jup}}$ . The rapid breakdown of the system in less than 10 kyr would only be guaranteed with masses as high as  $M_b = 33M_{\text{Jup}}$  and  $M_c = 45M_{\text{Jup}}$ ;
- For  $i = 15^\circ$  and all  $\Omega = 0^\circ$ – $180^\circ$ , the system with nominal masses is always stable over 100 Myr;
- For  $i = 30^\circ$ , the system with nominal masses is unstable for  $\Omega = 40^\circ$ – $75^\circ$  and stable otherwise.

## 5. Dynamical interaction between the planetesimal belts and the planets

To check where the outer and inner planetesimal belts (maintaining dust rings d and b) would be truncated by planets, we have picked up one exemplary angle configuration from within the “stability spot” seen in Fig. 8. The point chosen is  $(i, \Omega) = (30^\circ, 10^\circ)$ , which implies initial semimajor axes of 74.7, 41.8 and 24.6 AU for HR8799 b, c and d, respectively.

We launched 1000 massless planetesimals with uniformly distributed orbital elements ( $e_p = 0$ – $0.2$ ,  $i_p = 0$ – $10^\circ$ ,  $\{\omega_p, \Omega_p, M_p\} = 0$ – $360^\circ$ ). Of these, 200 planetesimals were initially confined to a ring between  $a_{\text{inner}} = 10$ – $20$  AU and the other 800 between  $a_{\text{outer}} = 90$ – $130$  AU. We integrated their orbits over 100 Myr with an accuracy of  $10^{-12}$  for low and nominal planetary masses, as given in Table 4. The high mass case was excluded, because the stability of companions themselves at  $(i, \Omega) = (30^\circ, 10^\circ)$  was only marginal.

Figure 12 shows that both the inner part of the outer ring and the outer part of the inner ring are swiftly cleared by the adjacent

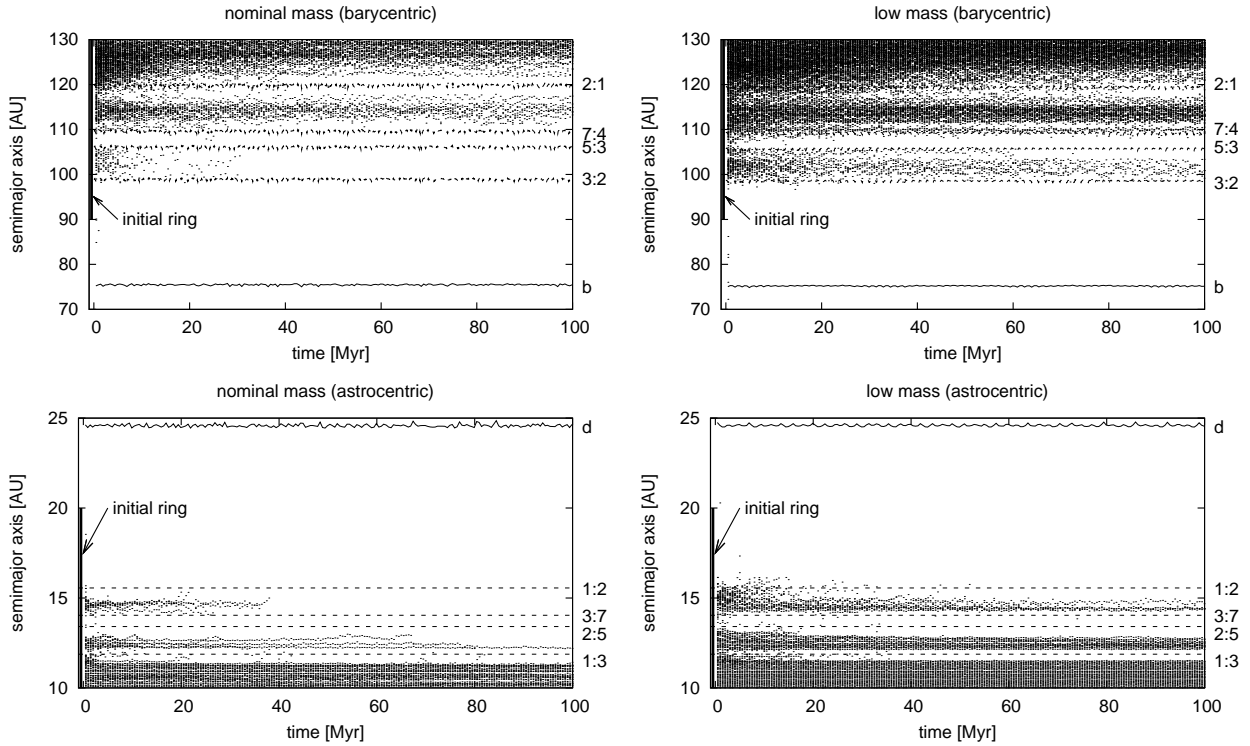


**Fig. 12.** Evolution of semimajor axes of planetesimals over 100 Myr for the nominal (*left*) and low (*right*) planet masses. Starting planetesimal rings are shown with vertical bars. Solid and dashed lines represent the location of planets and important resonances, respectively. Note that the outer ring (*top*) is plotted in barycentric osculating elements and the inner ring in astrometric ones. This choice leads to a sharper visibility of the resonance positions.

planet (b and d, respectively). The belt of remaining planetesimals develops “Kirkwood gaps” at the positions of major resonances. Over tens of Myr, the gaps get progressively more pronounced. Simultaneously, the fraction of particles surviving between them gradually decreases. As expected, the survival probability of planetesimals at a given distance is larger for lower masses of the companions.

For both rings and for the nominal- and low-mass cases, Fig. 13 presents the fraction of planetesimals that survived after 100 Myr in orbits with different initial semimajor axes. For nominal planetary masses, the outer ring shows a considerable depletion, with only  $\sim 10$  to 20% planetesimals surviving even outside 120 AU. There are almost no survivors inside the 5:3 and 7:4 resonances with HR8799 b at  $\approx 105$ –110 AU. In the low-mass case the survival fraction in the outer ring is appreciably higher (15–70% between  $\approx 110$ –130 AU). The inner ring retains 80–100% of planetesimals inside 11 AU. The outer edge of the ring is at 13 AU (nominal-mass planet) to 15 AU (low-mass one).

These results have to be compared with dust locations found from the SED fitting in section 3.2. As noted there, the far-infrared to millimeter part of the SED requires dust in the outer ring as close as 120 AU from the star; we have just shown that a significant fraction of planetesimals survives outside 120 AU after 100 Myr, at least in the low-mass case. In the nominal-mass case, the fraction of survivors is lower, but any firm conclusions appear premature, since the location of the outer ring is in fact not well-constrained (see section 3.2.). Next, the IRS spectrum interpretation requires dust in the inner ring at least at 10 AU away from the star. This is comfortably within the stability zone inside the orbit of HR8799 d for both the nominal-mass and low-mass cases. Moreover, 10 AU quoted above is the distance where

dust is required; as discussed in section 3.2, the parent planetesimals would orbit closer to the star, being yet safer against the perturbations of the innermost planet than their dust. In summary, our analysis of the outer system might slightly favor the low-mass case, but would not really pose any additional strong constraints to the planetary masses.

## 6. Conclusions and discussion

### 6.1. Conclusions

In this paper, we made an attempt of a coherent analysis of various portions of observational data currently available for the system of a nearby A5 star HR8799, which hosts debris dust as well as three planetary candidates recently discovered via direct imaging (Marois et al. 2008). A dedicated analysis of all known components of the system (the central star, imaged companions, and dust) leads us to a view of a complex circumstellar system (Fig. 14). It contains at least three planets in nearly-circular coplanar orbits bordered by two dust-producing planetesimal belts, one outside the planetary region and another inside it. Each planetesimal belt is encompassed by a dust disk. The outer dust disk may have a considerable extension, perhaps several hundreds of AU.

Our specific conclusions are as follows:

1. With previous estimates of stellar age ranging from  $\approx 20$  to  $\approx 1100$  Myr, high luminosity of observed cold dust may favor younger ages of  $\lesssim 50$  Myr. A younger age would automatically lower the masses for all three companions, estimated through evolutionary models, making the masses

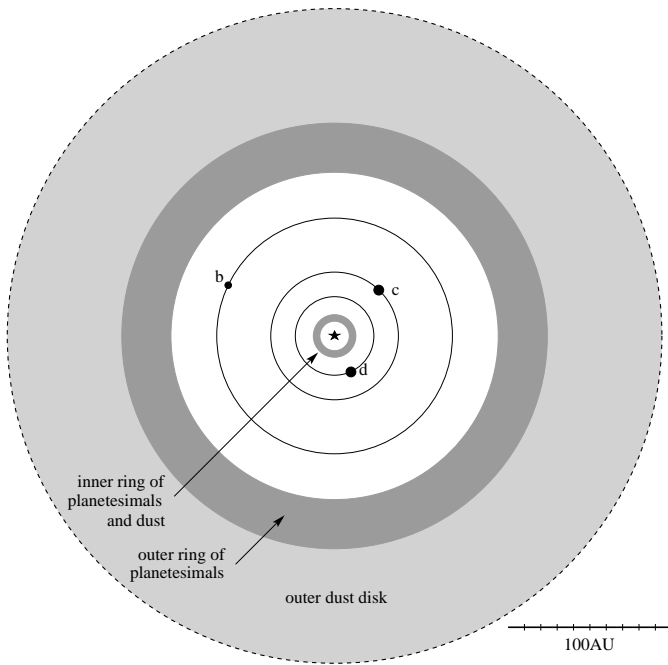


**Fig. 14.** A schematic view of the system HR8799.

more consistent with dynamical stability results (see conclusion 5).

2. The system is seen nearly pole-on. Our analysis of the stellar rotational velocity suggests an inclination of  $13 - 30^\circ$ , whereas  $i \geq 20^\circ$  seems to be mandatory for the system to be dynamically stable (see conclusion 5). Thus we arrive at a probable inclination range of  $20 - 30^\circ$ .
3. Our analysis of the available mid-infrared to millimeter photometry and spectrophotometry data reveals the presence of two dust rings, and therefore two parent planetesimal belts, an “asteroid belt” at  $\sim 10$  AU and a “Kuiper belt” at  $\geq 100$  AU. The dust masses are estimated to be  $\approx 1 \times 10^{-5} M_\oplus$  and  $4 \times 10^{-2} M_\oplus$  for the inner and outer ring, respectively.
4. Assuming that the system is indeed rather young ( $\lesssim 50$  Myr) and based on the photometry of the companions reported by Marois et al. (2008), our estimates with several evolutionary models suggest the masses of the companions to be lower than 7 to  $10 M_{\text{Jup}}$ .
5. We show that all three planets may be stable in the mass range suggested in the discovery paper by Marois et al. 2008 (between 5 and  $13 M_{\text{Jup}}$ ), but only for some of all possible orientations. For  $(M_b, M_c, M_d) = (5, 7, 7) M_{\text{Jup}}$ , an inclination  $i \geq 20^\circ$  is required and the line of nodes of the system’s symmetry plane on the sky must lie within  $0^\circ$  to  $50^\circ$  from north eastward. For higher masses  $(M_b, M_c, M_d)$  from  $(7, 10, 10) M_{\text{Jup}}$  to  $(11, 13, 13) M_{\text{Jup}}$ , the constraints on both angles are even more stringent. The stability of the two inner planets is due to locking in the 2:1 mean-motion resonance, and the stability of the outer couple is supported by the 2:1 commensurability, too. However, in many stable cases only one of the two resonances is strong. Another one is often shallow, with a circulating rather than librating resonant argument. For “wrong” orientations, the stability only seems possible with planetary masses lower than most evolutionary models would predict even for the youngest possible age (cf. Table 3). Should this be the case, this would necessitate revisions to the models.

6. Both dust/planetesimal belts appear to be dynamically stable against planetary perturbations, provided the masses of companions are such that they themselves are dynamically stable against mutual perturbations.

## 6.2. Prospects for future observations

Given the paucity of observational data available to date, many of the quantitative estimates listed above are quite uncertain and should be taken with caution. However, there is little doubt that new observations will arrive soon, verifying these estimates and on any account reducing the uncertainties.

Firstly, new observations of the planets themselves are expected and would be of great value. Better astrometry, and therefore a better determination of the orbits should become possible with improving instruments and methods of astrometric observations, and because of the longer time spans. Next, new photometry observations are needed. The companions are detected so far in JHK and L’. The SED is relatively flat in this wavelength range for objects with temperature of roughly 500 to 1500 K. Imaging photometric detections of the companions in either Gunn z ( $1 \mu\text{m}$ ) or M ( $5 \mu\text{m}$ ) must be possible with 8 to 10m class telescopes. They would allow one to constrain the objects’ temperature, because the colors z-J and L-M and their differences depend on temperature strongly over the relevant range of 500 to 1500 K. Further, spatially resolved spectroscopy of the companions may be possible with VLT/Sinfoni or Subaru/IRSC, but would be very challenging. If successful, it would place tighter constraints on temperature and gravity and, hence, radius and mass of the companions.

Secondly, new data on the dust portion of the system would be particularly promising. For instance, a better mid-infrared photometry would result in more reliable dust mass and location of the inner dust belt (“exozodi”). One could also think of near- and mid-IR interferometry observations, which have proven very successful not only for exozodi studies, but also for stellar radius determination (see, e.g., Di Folco et al. 2004; Absil et al. 2006; Di Folco et al. 2007; Absil et al. 2008). While HR8799 is too faint to be observed with the presently operating CHARA/FLUOR and Keck Interferometry Nuller instruments (e.g. for CHARA the K-magnitude of  $\lesssim 4$  mag is needed, whereas HR8799 has  $K = 5.2$  mag), this should become possible in the near future, for instance with VLTI/PIONIER and the LBTI Nuller. More observational effort is required for the outer disk as well. Resolving the outer debris disk, especially in scattered light, would answer several key questions at a time. On the one hand, it would further constrain the inclination of the entire system and the orientation of its line of nodes on the sky plane, drastically reducing the parameter space assumed in the dynamical simulations. On the other hand, the precise location of the inner rim of the disk could place a direct upper limit on the mass of HR8799 b, much in the same way it was recently done for the Fomalhaut planet (Kalas et al. 2008; Chiang et al. 2009). Since a high dustiness of the debris disk of HR8799 makes it a relatively easy target, whereas advantages of resolving it are obvious, success can be expected in the near future<sup>4</sup>.

Once the location and masses of the dust belts are better constrained from observations, it will become possible to access the position, masses, and other properties of directly invisible plan-

<sup>4</sup> After submission of this paper, we became aware of recent successful observations: the outer disk of HR8799 was resolved at 24 and  $70 \mu\text{m}$  with Spitzer/MIPS (Kate Su, pers. comm). The data analysis is ongoing.

esimal belts that produce and sustain that dust. This could be done with the help of elaborate collisional models (Krivov et al. 2008). The results could provide additional clues to the formation history of the system.

### 6.3. Origin and status of the system

The HR8799 system is among a few systems known to date to possess more than one planet *and* at least one planetesimal/dust belt. Other examples are HD38529 (Moro-Martín et al. 2007) and HD69830 (Beichman et al. 2005; Lisse et al. 2007). Further, it is not the only system with directly imaged companions whose masses most likely fall into the “planetary” (as opposed to brown dwarf) range. However, in some sense HR8799 does appear unique for the moment. The orbits of companions extending up to  $\approx 70$  AU are large, and their masses most likely too – probably almost at the limit of their dynamical stability against mutual perturbations. Even though we strongly argue that the masses are well below the deuterium burning limit, it is not clear whether the companions have formed in a “planetary” way (from the protoplanetary disk) or “stellar” way (as a multiple stellar system). In this sense, it remains questionable whether we are dealing with “true” planets. An argument in favor of the “stellar” formation would be, for instance, a low metallicity ( $\text{Fe}/\text{H} \approx -0.47$ , Gray & Kaye 1999), atypical of — although not the lowest among — the known planet host stars. The low metallicity is particularly unusual for a system with several high-mass planets. “Planetary” way of formation *in situ* could be feasible through the gravitational instability (GI) (Cameron 1978; Boss 1998). For GI to work, the density of the protoplanetary disk should exceed the Toomre density (Toomre 1964). At the same time, it should be low enough to allow efficient cooling, which is required for a disk to fragment into bound clumps (Gammie 2001). Both radiative and convective cooling rates may not be efficient enough for direct formation of giant planets by GI within several tens of AU from the parent star (Rafikov 2005, 2007). As far as the standard core accretion scenario is concerned, the only possibility to explain the formation of planets with several Jupiter masses would be to admit that they have formed closer to the star and then were scattered gravitationally to wider orbits (e.g. Veras & Armitage 2004). Nevertheless, it is difficult to find a mechanism that has circularized their orbits subsequently. Alternatively, massive planets formed by core accretion could have smoothly migrated from their birth places outward. However, this would require displacing a comparable – and therefore an unrealistically large – mass of planetesimals inward over large distances, rendering this mechanism problematic. Thus, by and large it remains unclear how the planets have formed. The era of directly imaged extrasolar planets that has just begun must eventually bring answers to these and many other questions.

*Acknowledgements.* We thank the referee, Daniel Fabrycky, for an insightful and very useful review, which greatly helped to improve the paper. AK and RN acknowledge discussions with Cesary Migaszewski on the dynamics of planets. SF and SM are funded by the graduate student fellowships of the Thuringia State. TOBS acknowledges support from *Evangelisches Studienwerk e.V. Villigst*. Part of this work was supported by the *Deutsche Forschungsgemeinschaft*, DFG project numbers Kr 2164/5-1, Kr 2164/8-1, Ne 515/13-1, Ne 515/13-2, and Ne 515/23-1, by the *Deutscher Akademischer Austauschdienst* (DAAD), project D/0707543, and by the International Space Science Institute in Bern, Switzerland (“Exozodiacal Dust Disks and Darwin” working group, <http://www.issibern.ch/teams/exodust/>).

## References

- Absil, O., di Folco, E., Mérand, A., et al. 2006, *A&A*, 452, 237  
 Absil, O., di Folco, E., Mérand, A., et al. 2008, *A&A*, 487, 1041  
 Allende Prieto, C. & Lambert, D. L. 1999, *A&A*, 352, 555  
 Baraffe, I., Chabrier, G., & Barman, T. 2008, *A&A*, 482, 315  
 Baraffe, I., Chabrier, G., Barman, T. S., Allard, F., & Hauschildt, P. H. 2003, *A&A*, 402, 701  
 Beichman, C. A., Bryden, G., Gautier, T. N., et al. 2005, *ApJ*, 626, 1061  
 Beichman, C. A., Neugebauer, G., Habing, H. J., Clegg, P. E., & Chester, T. J., eds. 1988, *Infrared astronomical satellite (IRAS) catalogs and atlases. Volume 1: Explanatory supplement, Vol. 1*  
 Boss, A. P. 1998, *ApJ*, 503, 923  
 Burrows, A., Marley, M., Hubbard, W. B., et al. 1997, *ApJ*, 491, 856  
 Cameron, A. G. W. 1978, *Moon and Planets*, 18, 5  
 Chabrier, G., Baraffe, I., Allard, F., & Hauschildt, P. 2000, *ApJ*, 542, 464  
 Chabrier, G., Baraffe, I., Allard, F., & Hauschildt, P. H. 2005 [arXiv:astro-ph/0509798]  
 Chambers, J. E. 1999, *MNRAS*, 304, 793  
 Chen, C. H., Sargent, B. A., Bohac, C., & et al. 2006, *ApJS*, 166, 351  
 Chiang, E., Kite, E., Kalas, P., Graham, J. R., & Clampin, M. 2009, *ApJ*, 693, 734  
 Close, L. M. & Males, J. R. 2009, *ApJ*, submitted [arXiv:0904.3936]  
 Cohen, M., Wheaton, W. A., & Megeath, S. T. 2003, *AJ*, 126, 1090  
 Di Folco, E., Absil, O., Augereau, J.-C., et al. 2007, *A&A*, 475, 243  
 Di Folco, E., Thévenin, F., Kervella, P., et al. 2004, *A&A*, 426, 601  
 Fabrycky, D. C. & Murray-Clay, R. A. 2008, *ApJ*, submitted [arXiv:0812.0011]  
 Fabrycky, D. C. & Winn, J. N. 2009, *ApJ*, 696, 1230  
 Fukagawa, M., Itoh, Y., Tamura, M., et al. 2009, *ApJ*, 696, L1  
 Gammie, C. F. 2001, *ApJ*, 553, 174  
 Goździewski, K. & Migaszewski, C. 2009, *MNRAS*, in press  
 Gray, R. O. & Kaye, A. B. 1999, *AJ*, 118, 2993  
 Hauschildt, P., Allard, F., & Baron, E. 1999, *ApJ*, 512, 377  
 Helou, G. & Walker, D. W., eds. 1988, *Infrared astronomical satellite (IRAS) catalogs and atlases. Volume 7: The small scale structure catalog, Vol. 7*  
 Høg, E., Fabricius, C., Makarov, V. V., et al. 2000, *A&A*, 355, L27  
 Jura, M., Chen, C. H., Furlan, E., et al. 2004, *ApJS*, 154, 453  
 Kalas, P., Graham, J. R., Chiang, E., et al. 2008, *Science*, 322, 1345  
 Kaye, A. B. & Strassmeier, K. G. 1998, *MNRAS*, 294, L35  
 Krivov, A. V., Löhne, T., & Sremčević, M. 2006, *A&A*, 455, 509  
 Krivov, A. V., Müller, S. amd Löhne, T., & Mutschke, H. 2008, *ApJ*, 687, 608  
 Lafrenière, D., Marois, C., Doyon, R., & Barman, T. 2009, *ApJ*, 694, L148  
 Laor, A. & Draine, B. T. 1993, *ApJ*, 402, 441  
 Lasker, B. M., Lattanzi, M. G., McLean, B. J., et al. 2008, *AJ*, 136, 735  
 Le Bouquin, J.-B., Absil, O., Benisty, M., et al. 2009, *A&A*, in press [arXiv:0904.1688]  
 Lisse, C. M., Beichman, C. A., Bryden, G., & Wyatt, M. C. 2007, *ApJ*, 658, 584  
 Marley, M. S., Fortney, J. J., Hubickyj, O., Bodenheimer, P., & Lissauer, J. J. 2007, *ApJ*, 655, 541  
 Marois, C., Macintosh, B., Barman, T., et al. 2008, *Science*, 322, 1348  
 Monet, D. G., Levine, S. E., Canzian, B., et al. 2003, *AJ*, 125, 984  
 Moór, A., Abraham, P., Drekas, A., et al. 2006, *ApJ*, 644, 525  
 Moro-Martín, A., Malhotra, R., Carpenter, J. M., et al. 2007, *ApJ*, 668, 1165  
 Moshir, M., Kopan, G., Conrow, T., & 9 colleagues. 1990, *IRAS Faint Source Catalogue, version 2.0*.  
 Pasinetti Fracassini, L. E., Pastori, L., Covino, S., & Pozzi, A. 2001, *A&A*, 367, 521  
 Paunzen, E. 2001, *A&A*, 373, 633  
 Perryman, M. A. C. & ESA, eds. 1997, *ESA Special Publication, Vol. 1200, The HIPPARCOS and TYCHO catalogues. Astrometric and photometric star catalogues derived from the ESA HIPPARCOS Space Astrometry Mission*  
 Rafikov, R. R. 2005, *ApJ*, 621, L69  
 Rafikov, R. R. 2007, *ApJ*, 662, 642  
 Rhee, J. H., Song, I., Zuckerman, B., & McElwain, M. 2007, *ApJ*, 660, 1556  
 Rodríguez, E. & Zerbi, F. M. 1995, *Inf. Bul. Var. Stars*, 4170, 1  
 Royer, F., Zorec, J., & Gómez, A. E. 2007, *A&A*, 463, 671  
 Sadakane, K. 2006, *PASJ*, 58, 1023  
 Sadakane, K. & Nishida, M. 1986, *PASP*, 98, 685  
 Schmidt, T. O. B., Neuhäuser, R., & Seifahrt, A. 2009 [arXiv:0905.0439]  
 Skrutskie, M. F., Cutri, R. M., Stiening, R., et al. 2006, *AJ*, 131, 1163  
 Song, I., Caillault, J.-P., Barrado y Navascués, D., & Stauffer, J. R. 2001, *ApJ*, 546, 352  
 Stevenson, D. J. 1982, *Planet. Space Sci.*, 30, 755  
 Su, K. Y. L., Rieke, G. H., Misselt, K. A., et al. 2005, *ApJ*, 628, 487  
 Su, K. Y. L., Rieke, G. H., Stansberry, J. A., et al. 2006, *ApJ*, 653, 675  
 Sylvester, R. J., Skinner, C. J., Barlow, M. J., & Mannings, V. 1996, *MNRAS*, 279, 915  
 Thébault, P. & Augereau, J.-C. 2007, *A&A*, 472, 169

- Toomre, A. 1964, *ApJ*, 139, 1217
- Turcotte, S. 2002, *ApJ*, 573, L129
- Uesugi, A. & Fukuda, I. 1982, *Catalogue of stellar rotational velocities* (revised)  
(Kyoto: University of Kyoto, Department of Astronomy, 1982, Rev.ed.)
- Veras, D. & Armitage, P. J. 2004, *MNRAS*, 347, 613
- Williams, J. P. & Andrews, S. M. 2006, *ApJ*, 653, 1480
- Wuchterl, G. 2001, in *IAU Symposium, Vol. 200, The Formation of Binary Stars*,  
ed. H. Zinnecker & R. Mathieu, 492
- Zacharias, N., Monet, D. G., Levine, S. E., et al. 2004, in *Bull. Amer. Astron.  
Soc.*, Vol. 36, 1418
- Zerbi, F. M., Rodríguez, E., Garrido, R., et al. 1999, *MNRAS*, 303, 275
- Zuckerman, B. & Song, I. 2004, *ApJ*, 603, 738